Residual Circulations Due to Bottom Roughness Variability under Tidal Flows

THOMAS F. GROSS AND FRANCISCO E. WERNER*

Skidaway Institute of Oceanography, Savannah, Georgia

(Manuscript received 21 June 1993, in final form 9 September 1993)

ABSTRACT

Tidal flows over irregular bathymetry are known to produce residual circulation flows due to nonlinear interaction with gradients of depth. Using the depth-averaged vorticity equations, the generation of residual vorticity and residual flows due to variation of the frictional coefficient are examined. The authors find that the contribution due to bottom roughness variations can be as large as that arising from gradients of depth and velocity. Specific cases are considered on the northern California shelf, Georges Bank, and the U.S. South Atlantic Bight.

The generation of residual vorticity is a strong function of the length scales at which roughness or depth vary. Length scales of bottom roughness variation are commonly within the range of greatest effect (e.g., sand patchiness, cobbly outcrops, etc.). The site-specific cases show that the bottom roughness variability can generate as much residual circulation as that expected from depth variability. The implication for numerical modeling studies is that resolution of roughness variability is as important as resolution of topography at length scales comparable to the tidal excursion. Therefore higher-resolution models that seek to resolve flow patterns due to tidal scale topographic variability will also require similarly resolved bottom roughness variability.

1. Introduction

Nonlinear interactions between tidal flows and spatially variable frictional effects generate mean currents and overtides. Differential shear produced within the tidal stream arising from spatial frictional gradients gives rise to vorticity. Locally, the vorticity production is symmetric upon the returning tide and thus no net vorticity is generated. However, the Lagrangian view shows that continuous decay of the vorticity away from the source prevents the return of generated vorticity. Hence there is a net flux through the generation site, which will separate regions of positive and negative vorticity thus creating residual flows. Detailed discussions found in Huthnance (1973), Zimmerman (1978, 1981), Loder (1980), and Robinson (1983) consider cases where the frictional variability—and the ensuing vorticity and residual circulation field generation—is induced by topographic variations. In this paper we extend these analyses, building on the approach introduced by Robinson (1983), and examine the effect of variable bottom roughness as a generation mechanism for horizontal shear. We identify conditions under which spatial gradients in bottom roughness can be as important as topographic variations in generating residual flows.

Circulation models of shallow seas and shelves are limited at some level by spatial resolution. While topographic variations within the limits of resolution are responsible for advective and planetary vorticity steering, subgrid-scale variations of topography are expected to produce horizontal momentum and tracer diffusivity (Abraham et al. 1987). A study by Abraham and Gerritsen (1990) showed that subgrid-scale diffusion arising from variability in bottom topography irregularities cannot be assumed to be constant.

The importance of including accurate topography in circulation models has been recognized for some time. However, most models still use spatially constant bottom boundary conditions derived from turbulent boundary-layer models such as linear or quadratic drag coefficient formulations. These formulations assume that the bed is uniformly rough. Side scan sonar images of topographically simple regions of the continental shelf have revealed considerable variability in the bed characteristics. For example, on the northern California shelf, regions of exposed cobbles and large rock outcrops are juxtaposed with sand belts covered with ripples or areas of mud with intensively bioturbated surfaces (Cacchione et al. 1983; Wheatcroft 1994). While the conversion of side scan sonar images and photographs of these features cannot, as yet, be used to derive precise drag coefficient estimates they do demonstrate that bottom roughness variability is common and can be expected to play a role in circulation patterns.

* Current affiliation: Marine Sciences Program, University of North Carolina, Chapel Hill, North Carolina.

Corresponding author address: Dr. Thomas F. Gross, Skidaway Institute of Oceanography, 10 Ocean Science Circle, Savannah, GA 31411. E-mail: tom@skio.peachnet.edu

2. Equation development

An equation for the Lagrangian rate of change of vorticity will be derived including the term that results from spatially variable coefficient of bottom friction. The depth-averaged two-dimensional momentum equation is

$$\frac{\partial \mathbf{U}}{\partial t} + (\mathbf{U}\cdot\nabla_h)\mathbf{U} + f\times\mathbf{U} = -\frac{\nabla_h p}{\rho} - \frac{k_f}{h+\zeta}\mathbf{U}|\mathbf{U}|, \tag{1}$$

where using standard notation, $\mathbf{U}$ is the depth-averaged horizontal velocity vector, $|U|$ is the depth-averaged speed, t is time, f is the Coriolis term, $\nabla_h p$ is the horizontal pressure gradient, ρ is density, $h+\zeta$ is depth plus surface displacement, and k_f is the bottom friction coefficient. Taking the curl of the depth-averaged momentum equation, the Lagrangian equation for vorticity, $\omega = \nabla\times\mathbf{U}$, is

$$\frac{d\omega}{dt} = -\frac{k_f|\mathbf{U}|}{h+\zeta}\omega + \frac{(f+\omega)}{(h+\zeta)}\frac{d(h+\zeta)}{dt} + \frac{k_f\mathbf{U}|\mathbf{U}|}{h+\zeta}\times\left[\frac{\nabla|\mathbf{U}|}{|\mathbf{U}|} - \frac{\nabla(h+\zeta)}{(h+\zeta)} + \frac{\nabla k_f}{k_f}\right]. \tag{2}$$

The last four terms are the vorticity production terms: topographic vortex stretching "Coriolis mechanism," differential velocity torque "velocity gradient mechanism," torque due to gradient in depth-distributed friction "depth gradient mechanism," and the contribution to vorticity due to gradients in the friction coefficient "roughness-gradient mechanism." The first three are discussed by Robinson (1983). The roughness gradient mechanism contribution will be compared to the other source terms. If the coefficient

$$\frac{k_f\mathbf{U}|\mathbf{U}|}{h+\zeta}$$

can be held constant for small gradients of $|U|$, $(h+\zeta)$, and k_f, then the relative effects of all three gradients can be compared. However, because the problem is nonlinear, the constancy of

$$\frac{k_f\mathbf{U}|\mathbf{U}|}{h+\zeta}$$

and the independence of $|\mathbf{U}|$, $(h+\zeta)$ and k_f cannot be a priori asserted.

The k_f used here is a depth-averaged velocity-based friction term, which is only loosely identified with true turbulent boundary-layer processes. However, we can derive a relationship to the bed roughness parameter, z_o, by assuming a constant drag law due to a logarithmic boundary layer:

$$U(z) = \frac{u_*}{\kappa}\ln\frac{z}{z_o} \tag{3}$$

$$\frac{\tau_z}{\rho} = u_*^2 = C_d U_{100}^2 \tag{4}$$

$$C_d = \left(\frac{1}{\kappa}\ln\frac{100\text{ cm}}{z_o}\right)^{-2}, \tag{5}$$

where κ is von Kármán's constant, τ_z is bottom bed stress, and U_{100} is the speed 1 m above the bottom. The difference between k_f and C_d is the factor of $(U_{100}/|U|)^2$, which is of order one. Therefore we will identify k_f with C_d in order to cast the dependence of spatial variability of k_f in terms of spatial variability of the roughness parameter z_o:

$$\frac{\nabla k_f}{k_f} = \frac{\nabla C_d}{C_d} = \frac{\nabla\left[\frac{1}{\kappa}\ln\frac{100}{z_o}\right]^{-2}}{\left[\frac{1}{\kappa}\ln\frac{100}{z_o}\right]^{-2}} = \frac{2}{\ln\frac{100}{z_o}}\frac{\nabla z_o}{z_o}. \tag{6}$$

The roughness parameter z_o has been identified with physical bed roughness as well as with the effects of sediment transport, stratification, and wave–current interaction (Grant and Madsen 1986). Direct field estimates have shown that z_o can vary by an order of magnitude or more if dynamic effects such as waves and stratification are active. Throughout this paper we consider variations of a factor of two as probable variability given general observations of bed morphology and sediment type. Equation (6) shows that the roughness-gradient mechanism term is multiplied by $2/\ln(100/z_o)$. If $z_o \approx 1$ cm the factor is 0.4. Therefore a 50% change in z_o produces the same residual vorticity as that caused by a 20% change in depth.

3. Mechanism

A Lagrangian description of residual vorticity generation is provided by Robinson (1981). Consider a flow over a localized region of vorticity generation. Over a tidal cycle, as the fluid moves past the source region it advects locally acquired (positive or negative) vorticity while losing some vorticity due to dissipation. Upon its return to the source region from the opposite direction the fluid picks up vorticity of the opposite sign. Although the Lagrangian time-averaged vorticity of a fluid parcel is zero (or close to zero), the spatial distribution of the vorticity field is nonzero. We refer to this as the residual vorticity. Robinson (1983) describes mechanisms for the generation of residual vorticity and residual circulation by fluctuating (e.g., tidal) currents over ridges due to the stretching and shrinking of the fluid columns and due to frictional effects. Both mechanisms require that there be a flow component normal to the axis of the topographic feature; that is, to first order the mechanisms will not result in mean

vorticity/residual current generation if the oscillating flow is parallel to the ridge or bank.

The bottom-friction generation mechanism, arising from variations in (or patches of) bottom roughness, torques the fluid element straddling regions of smooth and rough bottom (Fig. 1). Four scenarios can occur, including the dependence on the direction of the flow impinging on the roughness patches and whether the roughness patch is more (or less) rough than its surroundings. Figure 1 shows the resulting residual vorticity and currents.

The mechanisms of Coriolis, depth gradient, and roughness gradient can act to reinforce or weaken the total vorticity generation dependent on flow orientation and distribution of roughness on or off the bank. The Coriolis mechanism always produces anticyclonic vorticity for flow across a bank. Maximum generation of vorticity/residual current occurs when the anticyclonic vorticity produced by the Coriolis mechanism is reinforced by flow oriented with the shallow side on its right [from the depth gradient mechanism; Robinson (1983), Fig. 7.4 and 7.5] and a bank relatively rougher than the ambient (from the roughness-gradient mechanism, Fig. 1b). The combination of Coriolis and depth gradient mechanisms was identified by Huthnance (1973) and Robinson (1983) to be consistent with the observed preferred sandbank orientation, suggesting feedback from the residual current system to the process of sandbank growth. The inclusion of the effect of variations in roughness suggests that the roughness on the bank must be greater than that of the ambient roughness, for example, a sandbank roughened by ripples surrounded by a smoother domain, to generate the largest residual circulation.

4. Residual vorticity: Scale analysis

The spatial distribution of vorticity, the Eulerian field, is controlled by length scales of advection, distribution of sources, and the time scale of dissipation. An estimate of the magnitude of the residual vorticity generation by the roughness-gradient mechanism relative to the Coriolis and depth gradient mechanisms will be obtained by extending the approach introduced by Robinson (1983). An Eulerian description of residual vorticity generation can be obtained with additional simplification of Eq. (2) by neglecting the effects of the tidal elevation and other small terms. We need only identify velocity scales and the length scales parallel and normal to the flow associated with the variations in depth and in bottom roughness. Solving for residual vorticity induced by narrow tidal current ellipses, $\vec{U} = V\cos\sigma t$, where V is the tidal current amplitude and σ is the tidal frequency, we obtain three vorticity-generating terms, A, B, and B', and a damping term, C:

$$A(s) = \frac{f}{h} V \frac{\partial h}{\partial s} \tag{7a}$$

$$B(s) = k_f V \frac{\partial}{\partial n}\left(\frac{V}{h}\right) \tag{7b}$$

$$B'(s) = \frac{V|V|}{h}\frac{\partial k_f}{\partial n} \tag{7c}$$

$$C(s) = \frac{k_f V}{h}, \tag{7d}$$

where s and n are streamwise and normal directions. A spatial decomposition of the terms A, B, and B' reveals the time dependence of their contributions to vorticity generation throughout the tidal cycle. Numerical solutions are obtained by time stepping the equations through many tidal oscillations (at least 10) until the solution becomes independent of initial conditions. The net vorticity generation due to each term A, B, and B' is modulated by factors $I(W_m)$, $I(Y_m)$, and $I(Y'_m)$, which depend upon the tidal excursion length E, and the geomorphological length scales [also expressed by Robinson (1983) as wavenumber $k_i = 2\pi/\Delta L$]: ΔL_h the spatial scale of depth variation, and ΔL_k the spatial scale of bottom roughness variation:

$$\lambda_1 = \frac{C}{\sigma} = \frac{k_f V}{h\sigma} \tag{8a}$$

$$\lambda_{2h} = \frac{2\pi}{\Delta L_h}\frac{E}{2} \tag{8b}$$

$$\lambda_{2k} = \frac{2\pi}{\Delta L_k}\frac{E}{2}, \tag{8c}$$

as shown in Fig. 2. The magnitude of the λ_1 coefficient provides an indication of the bottom friction/dissipative effect; for example, for $\lambda_1 \approx 1$ or greater, frictional effects can be expected to be large and the $I(W)$ and $I(Y)$ become small. The λ_2 provide a ratio of the tidal excursion to the length scale over which topographic λ_{2h} (or bed roughness λ_{2k}) variations occur. Peak vorticity generation occurs when λ_{2h}, $\lambda_{2k} \approx 2$, which corresponds to either depth variation or roughness variation over length scales $\Delta L \approx (\pi/2)E$. The greatest generation of tidal residuals occurs when the field of varying roughness is approximately the same length as the tidal excursion.

5. Discussion

The vorticity generation by the roughness gradient mechanism is analogous to the velocity gradient and depth gradient mechanisms. All create a shear by dragging the water column more on one side than the other. The differential shearing is due to a difference in water column-averaged friction. While friction is usually presented in a simplified parameterized form, it is ac-

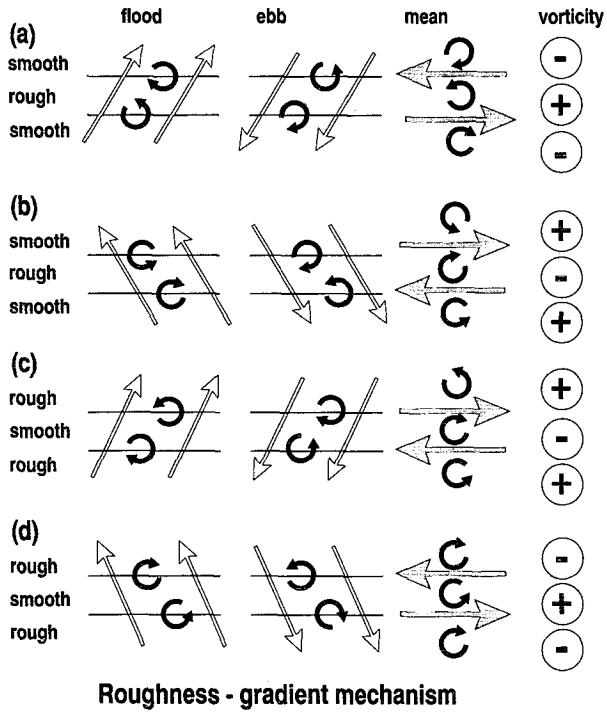

FIG. 1. Generation of residual vorticity due to the roughness-gradient mechanism.

tually the result of 3D turbulence generation by the rough seabed with the vertically sheared flow within the turbulent bottom boundary layer. This 3D turbulence spans very small length scales, O (mm), up to largest scales of order the bottom boundary-layer thickness of O (10 m). Usually friction coefficients are used to include the effects of unresolved 2D horizontal eddy motions that are much larger O (10s km). The implied (or explicit for numerical models) spatial averaging produces larger friction coefficients when larger space scales are used for the averaging. The larger friction factors are needed to include the effects of tidally induced vorticity. Our interest here is the generation of those 2D eddies by intermediate topographic and bed roughness variations of O (100 m–10 km).

In the absence of spatial averaging the friction coefficient will be described by the 3D boundary-layer turbulence. Transforming k_f into the roughness length scale z_o allows us to use observations of bed morphology to estimate the variability of the friction term [Eq. (6)]. At its simplest, z_o is related to the length scale of bed roughness, k_b, by the Nikuradse formula $z_o = k_b/30$. Although derived for the diameter of sand grains distributed uniformly over the interior of pipe flows, the relationship has been found to work well where the seabed is flat and k_b is the size of bottom roughness features such as sand ripples, cobbles, animal tracks, shells, and tubes, etc. (Perry et al. 1969). Simple formulations of ripple geometry to z_o have also been proposed (e.g., Wooding et al. 1973; Grant and Madsen 1982).

The next larger scales of bed roughness commonly encountered are sand waves and rocky bottoms where roughness scales are of order 1–10 m. Because a turbulent logarithmic region is only 1–10 m deep, the direct relation of drag coefficient to z_o and k_b is not valid. However, the effect on drag coefficient of increasing roughness is monotonic. At larger roughness scales the effect of obstacles on the flow is felt as form drag. At some point the effect on the mean flow of large roughness is the same as depth variation. Our investigation of frictional effects should stop before that point. Field observations of bottom roughness variability can be found in descriptions of bed morphology and sediment types. Few, if any, oceanic studies have included direct measurements of turbulence generation across roughness changes (Nowell 1983; Grant and Madsen 1986). However, see Wieringa (1993) for a review within the meteorological literature.

In Table 1 we compare the relative importance of vorticity generation by the roughness gradient mechanism to the other mechanisms for various field situations. The table presents scaling for several continental shelf situations where residual vorticity generation by tidal action may be significant. Excluded from Table 1 are areas where the depth is too great. Although near-bed secondary flows may be important to deep water tidal cases, the above analysis was based on depth-averaged effects inversely proportional to depth. Each case is characterized by a tidal velocity V, depth h, depth change Δh, bottom roughness z_o, and length scales of variation of the depth and roughness in both the streamwise and normal to stream directions ΔL_{hs}, ΔL_{hn}, ΔL_{ks}, and ΔL_{kn}. The variation of z_o is always

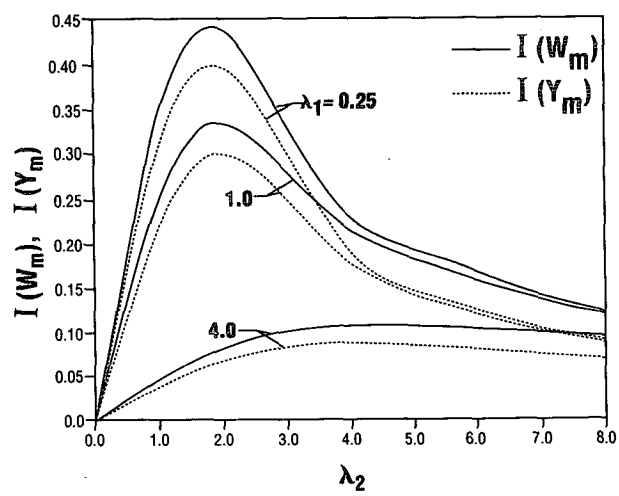

FIG. 2. Scale factors for the effectiveness of vorticity generation [$I(W_m)$, $I(Y_m)$; see Eqs. (8) and (9) in the text] as a function of frictional/dissipative effects (λ_1) and the ratio of the tidal excursion to the topographic or roughness length scale (λ_2). Adapted from Robinson (1983).

TABLE 1. Examples of the interaction of a semidiurnal (12.4 h) tide with various length and depth scales to derive estimates of the importance of the vorticity generation mechanisms. All units are MKS, except z_o, which is centimeters. The value of the Coriolis parameter is chosen as $f = 0.0001\ s^{-1}$.

	California		Georges Bank				South Atlantic Bight			
Site	Midshelf	Patch	North flank	South flank	Shoal	Sand wave	Midshelf	Gray's Reef	Wassaw Channel	Wassaw sand deposit
V	0.05	0.05	0.75	0.50	1.00	1.00	0.30	0.30	0.30	0.30
h	80	80	100	80	30	30	16	16	10	3
Δh	10.0	10.0	80.0	10.0	15.0	5.0	1.0	1.0	3.0	0.5
ΔL_{hs}	50 000	50 000	6000	25 000	30 000	200	1500	1500	3000	2000
ΔL_{hn}	1000	1000	25 000	50 000	3000	2000	5000	5000	500	1000
ΔL_{kn}	1000	1000	25 000	25 000	3000	2000	15 000	5000	500	3000
ΔL_{ks}	50 000	500	25 000	25 000	30 000	200	3000	3000	3000	3000
z_o-	0.25	0.25	0.25	0.25	0.50	0.50	0.25	2.00	0.50	0.25
z_o+	0.50	0.50	0.50	0.50	1.00	1.00	0.50	4.00	1.00	0.50
k_f	0.0051	0.0051	0.0051	0.0051	0.0066	0.0066	0.0051	0.0129	0.0066	0.0051
Δk_f	0.0012	0.0012	0.0012	0.0012	0.0018	0.0018	0.0012	0.0050	0.0018	0.0012
λ_1	0.02	0.02	0.27	0.23	1.57	1.57	0.68	1.73	1.41	3.61
λ_{2h}	0.04	0.04	5.59	0.89	1.49	223.56	8.94	8.94	4.47	6.71
λ_{2k}	0.04	4.47	1.34	0.89	1.49	223.56	4.47	4.47	4.47	4.47
$I(Y_{m'})$	0.014	0.014	0.133	0.287	0.200	0.004	0.078	0.075	0.149	0.081
$I(Y'_{m'})$	0.014	0.200	0.368	0.287	0.200	0.004	0.161	0.142	0.149	0.095
$I(W_m)$	0.016	0.016	0.178	0.322	0.226	0.005	0.111	0.105	0.186	0.106
$\frac{k_f V}{\sigma}\frac{\partial(V/h)}{\partial n}$	$2.0\cdot10^{-9}$	$2.0\cdot10^{-9}$	$0.87\cdot10^{-6}$	$0.08\cdot10^{-6}$	$52.4\cdot10^{-6}$	$0.46\cdot10^{-6}$	$0.20\cdot10^{-6}$	$0.49\cdot10^{-6}$	$38.0\cdot10^{-6}$	$14.5\cdot10^{-6}$
$\frac{V^2}{\sigma h}\frac{\partial k_f}{\partial n}$	$3.8\cdot10^{-9}$	$55.3\cdot10^{-9}$	$0.73\cdot10^{-6}$	$0.32\cdot10^{-6}$	$29.2\cdot10^{-6}$	$0.77\cdot10^{-6}$	$0.53\cdot10^{-6}$	$5.68\cdot10^{-6}$	$35.3\cdot10^{-6}$	$8.39\cdot10^{-6}$
$\frac{fV}{\sigma h}\frac{\partial h}{\partial s}$	$1.4\cdot10^{-9}$	$1.4\cdot10^{-9}$	$12.7\cdot10^{-6}$	$0.57\cdot10^{-6}$	$2.70\cdot10^{-6}$	$2.67\cdot10^{-6}$	$0.98\cdot10^{-6}$	$0.93\cdot10^{-6}$	$3.97\cdot10^{-6}$	$1.89\cdot10^{-6}$
V_{res}	0.000	0.000	0.068	0.002	0.093	0.019	0.002	0.003	0.020	0.008

given as a factor of 2, and the gradient determined by prescribed length scales, ΔL_{kn}, ΔL_{ks}. The values of k_f and Δk_f are calculated from z_o with Eqs. (5) and (6). The λ_1, λ_{2h}, and λ_{2k} values are calculated and used with the solution shown in Fig. 2 to produce $I(W_m)$, $I(Y_m)$, and $I(Y'_m)$. The vorticities associated with the four generation mechanisms are

$$\frac{k_f V}{\sigma}\frac{\partial(V/h)}{\partial n} \approx \frac{k_f V^2}{\sigma h^2}\frac{\Delta h}{\Delta L_{hn}} I(Y_m(\lambda_1, \lambda_{2h})) + \frac{k_f V}{\sigma h}\frac{\Delta V}{\Delta L_{hn}} I(Y_m(\lambda_1, \lambda_{2h})) \quad (9a)$$

$$\frac{V^2}{\sigma h}\frac{\partial k_f}{\partial n} \approx \frac{V^2}{\sigma h}\frac{\Delta k_f}{\Delta L_{kn}} I(Y'_m(\lambda_1, \lambda_{2k})) \quad (9b)$$

$$\frac{fV}{\sigma h}\frac{\partial h}{\partial s} \approx \frac{fV}{\sigma h}\frac{\Delta h}{\Delta L_{hs}} I(W_m(\lambda_1, \lambda_{2h})). \quad (9c)$$

The mechanisms are scaled by the effectiveness of the term at the length scale of variation due to λ_1, λ_{2h}, and λ_{2k}. The mechanisms of depth gradient and velocity gradient have been combined in (9a) and Table 1.

An estimate of the magnitude of the residual velocity, V_{res}, can be obtained from vorticity using the circulation theorem. Because the residual vorticity is distributed over an area that scales with tidal excursion E, the circulation theorem gives $V_{res} \propto \Omega E$ $(=\Omega 2V/\sigma)$ with a constant of proportionality that depends on geometry, assuming the far field velocity is zero. Here Ω is the vorticity from Eqs. (9a–c). For instance circulation around an isolated eddy with diameter E and uniform vorticity, Ω, is given by $\Omega\pi(E/2)^2 = \pi E V_{res}$. Flow over a uniform ridge will create a sheared flow whose residual velocity could be described by circulation around a square $\Omega E^2 = V_{res}E$. Notice V_{res} due to the velocity-, depth-, and roughness-gradient terms (all of which are proportional to V^2) depends on the cubic power of V. A small reduction in V due to the generation of V_{res} quickly reduces the production of V_{res}. This negative feedback is strongly present whenever estimates of V_{res} become large compared to V.

The values in Table 1 are rough estimates to provide insight to the regions and situations where residual vorticity may or may not be an important physical feature of the flow. Numerical estimates of vorticity and residual velocity obtained in this manner are subject to variability associated with prescribing the controlling length, time, and velocity scales. For example, residual velocity arising from the gradient mechanisms

is sensitive to the cubic power of the mean tidal current. The derivation of velocity from vorticity with the circulation theorem introduces a factor of up to 8 depending upon whether the vorticity value is considered to describe a circular eddy or a uniform velocity shear. The combination of these and other uncertainties can over- or underestimate the residual flows observed in nature. The results of the table are understood to be indications of relative magnitudes of the generation terms.

Table 1 provides examples of vorticity generation in several shallow environments. The northern California shelf is characterized by relatively weak tides and smooth topography on a steep shelf. In contrast Georges Bank has strong tides and complicated topography consisting of ridges, sand waves, steep slopes, etc. In the South Atlantic Bight example we examine the possibility of vorticity generation in the vicinity of tidal inlets and due to isolated rocky outcrops. While tidal velocities and topography of these three areas are well documented, the information to accurately describe the roughness variations is lacking. Therefore we estimate roughness values conservatively and use a factor of 2 variation of z_o when describing the roughness-gradient mechanism magnitude.

a. *Northern California shelf*

The northern California shelf is narrow and straight (Fig. 3a) and the relatively weak tides, which are predominantly alongshelf, are often overwhelmed by noctidiurnal winds (Rosenfeld and Beardsley 1987). In this region Cacchione et al. (1984) observed rippled scour depressions where areas of coarse sand with sand waves cut through a more uniform band of fine sand. These depressions are tens to hundreds of meters wide and 0.10–0.30 m deep and are filled with wave-formed sand ripples with 1–1.7 m wavelengths. The roughness change over the rippled fields is probably at least a factor of 10 while the depth changes are only a few percent. The shelf bottom is composed of bands of mud and sand 0.5 to 2.0 km wide, which are often marked by wave-formed ripples. These create approximate z_o roughness values varying from 0.15 cm to 1.0 cm due only to changes in sediment composition. In this area surface gravity waves interact with the bottom boundary layer to cause increased apparent roughness of z_o = 1.0–10.0 cm (Grant and Madsen 1979; Gross et al. 1992). However, the near-bed wave climate does not change very rapidly across the shelf (a factor of 2 change in near-bed orbital velocity of 14 sec waves would occur with a depth change from 100 m to 25 m over 8 km). The Table 1 midshelf example shows that for a factor of 2 change in z_o, or a 20% change of k_f, the generation of vorticity by the roughness gradient mechanism is comparable to that generated by the depth gradient mechanism. Because in this region the tides are small and the flow does not cross the gradients of z_o or h, the total vorticity generation is small and probably not observable. Where the tidal flow crosses the rippled scour depressions observed by Cacchione et al. (1984), the alongstream length scale of the roughness patch ΔL_{ks} is approximately 500 m (Table 1, Patch example). This increases the value of λ_{2k} to 4.5, indicating a better match between alongstream length scale of the roughness patch and tidal excursion. The roughness-gradient mechanism is increased by a factor of 15 over the uniform alongshore gradient cases. However, even in this case the estimated residual velocity is negligible. The main reason for the small residuals is the cubic relationship with the weak tidal velocity.

b. *Georges Bank*

Tidal velocities on Georges Bank reach magnitudes of the order of 1 m s^{-1} (Fig. 3b) and residual tidal velocities have been estimated at 0.1–0.2 m s^{-1} (see reviews in Backus 1987). Loder (1980) discusses the generation of the tidal residual velocities by Coriolis and continuity effects and the tidally rectified current interaction with the Stokes drift over the slopes of Georges Bank. We will consider the additional source of vorticity produced by roughness variations in this environment.

Georges Bank has dramatic bathymetry and is covered with a variety of bed forms (Twichell et al. 1987). The northern flank of Georges Bank is steep in the direction of the tidal flow, which is across isobaths, with a bottom slope of 1/75. The bottom roughness grades from medium to fine sands in the off-bank direction and probably varies little in the alongisobath direction (ΔL_n = 25 km). We characterize the roughness with z_o values of 0.25–0.5 cm changing gradually over 25 km in alongstream and cross-stream directions. Estimates in Table 1 show that the dominant generation term is the Coriolis mechanism as the flow crosses isobaths ($V_{res} \approx 7$ cm s^{-1} based on uniform shear vorticity geometry).

The southern flank of Georges Bank has weaker tidal currents and the sediment grades from medium to fine sands in the off-bank direction. It is of a gentler slope (1/2500) than the northern flank. Table 1 shows that with these gradients of depth and roughness there is little local generation of residual currents ($V_{res} \approx 0.15$ cm s^{-1} based on uniform shear vorticity geometry).

On the crest of Georges Bank there are many shoals constructed of sandy deposits (Twichell et al. 1987). The shoals are ridgelike structures 30 km long and about 3 km across oriented 5°–15° counterclockwise to the major axis of the tidal currents. The troughs between shoals are around 40 m deep and the shoals rise to within 10–20 m of the surface. The troughs between the sandy shoals are gravel lag. We conservatively describe the roughness gradient between the smooth sandy crests and rougher troughs with z_o values of 0.5–

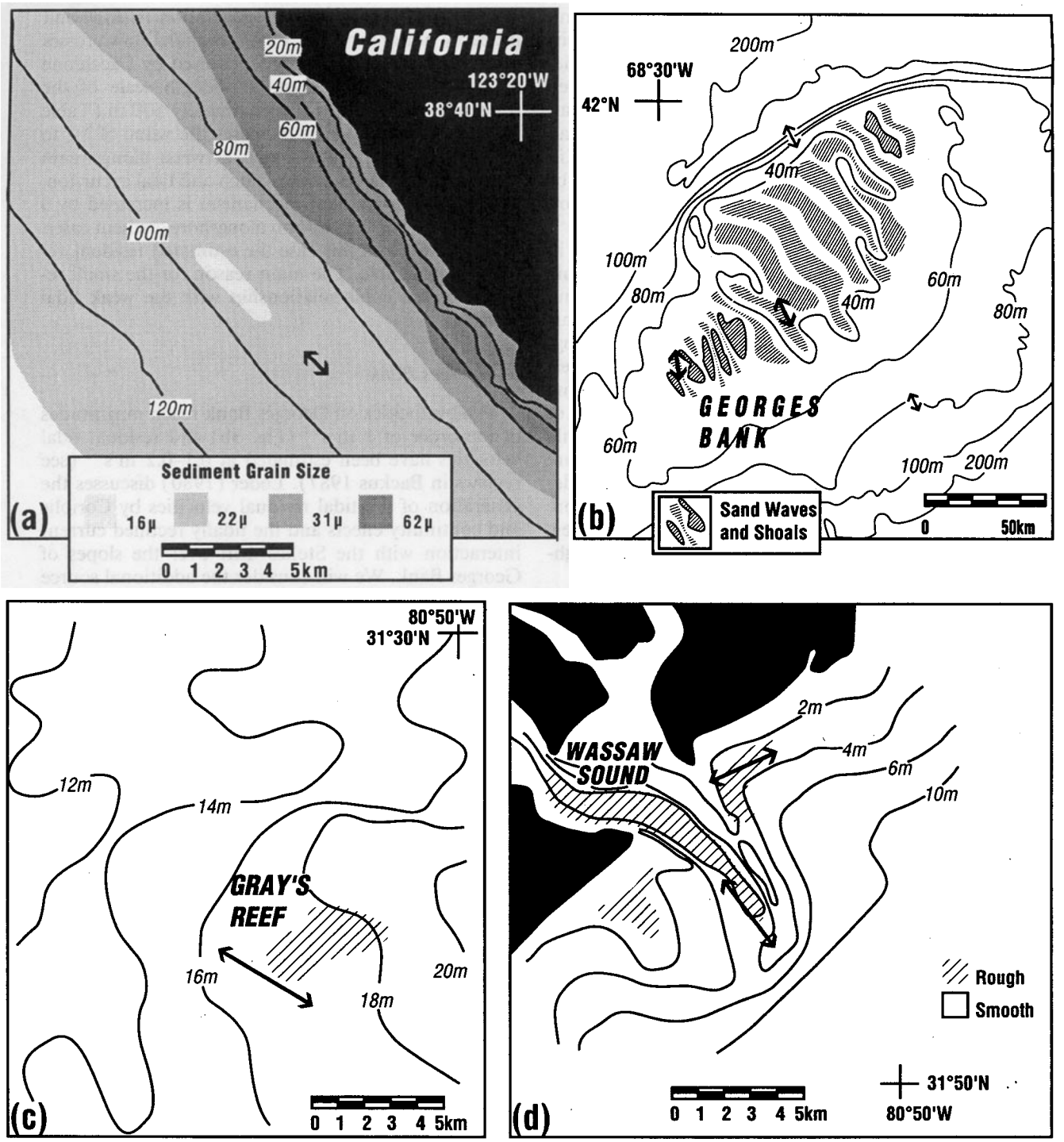

FIG. 3. Schematics of (a) northern California shelf (from Field et al. 1992); (b) Georges Bank; (c) South Atlantic Bight shelf and Gray's Reef; (d) Wassaw Sound. The tidal excursion length and major axis are indicated by the two-headed arrows.

1.0 cm. The tidal currents of 1.0 m s^{-1} give a tidal excursion of 14 km, which is $\approx 1/\pi$ times the length of the shoals. This means that the features are well tuned to generate residual vorticity. The largest generating term is the depth-gradient mechanism, but the roughness gradient mechanism is also large. The Coriolis mechanism is not as large because the flow is largely parallel to the shoals. The residual velocity generated for the shoals (assuming circular eddy geometry) is 9.3 cm s^{-1} or about 10% of the tidal velocity. This

may be too large for the perturbation approximation and smaller residuals are actually expected.

Over and between the shoals is a complex mosaic of sand waves (Jordan 1962). Those sand waves are often oriented crest-perpendicular to the flow. Most of the sand has been swept out of the troughs and concentrated on the ridges where a greater density of sand waves are found (Twichell et al. 1987). Between the shoals the sand waves are sediment starved, that is, between the sand waves the gravel bed is exposed. The residual circulation generated by 1 m s^{-1} tides flowing over the crests of sand waves 5 m high, 200 m wide, and 2 km long apparently is dominated by the Coriolis mechanism because the flow is across depth contours (Table 1). In spite of large slopes and gradients of roughness, the residuals produced by the sand waves are much smaller than that due to the shoals because the tidal excursion is many times greater than the length scale of the sand waves [$I(W_m)$ is small]. It might be appropriate to consider the sand waves as small-scale roughness elements for the circulation patterns around the shoals.

c. *South Atlantic Bight*

The South Atlantic Bight is a wide and shallow shelf of uniform characteristics with tidal currents of 20–30 cm s^{-1} and the main axis of the tidal ellipse oriented on/off shelf (Fig. 3c). Table 1 shows that the mean slope of the midshelf (1 m in 1500 m across shelf) is insufficient to generate significant residual vorticity. A gradient of z_o due to the transition from near-shore muds and clays to offshore relict sands (Δz_o = 0.25–0.5 cm) results in some vorticity generation (V_{res} = 0.2 cm s^{-1}, for uniform shear geometry). Throughout the shelf environment of uniform gradients there are occasional rock outcrops, such as the Gray's Reef National Marine Sanctuary (Henry 1985). The reef is a limestone outcrop of rock formations 1–2 m high covering a 2 km by 5 km area, about 30 km offshore. The drag coefficient due to 1–2 m rock outcrops should be large, $k_f \approx 0.01$. The correspondence of z_o to geometric bottom roughness of boulders, $z_o = k_b/30$, is not applicable because a logarithmic velocity profile would not be expected within 2 m of such a rugged bottom. Table 1 uses values of z_o chosen to give the large drag coefficient and again a roughness gradient is derived from a factor of 2 change in z_o. As tides sweep past the abruptly changing roughness of the reef, residual vorticity is generated that may impact the local flow field. In this case the vorticity generated by the roughness gradient mechanism is an order of magnitude greater than that generated by the velocity/depth-gradient or Coriolis mechanisms. The resultant circular eddy with $V_{res} \approx 0.3$ cm s^{-1} may not be easily observable.

Due to strong gradients in depth, velocity, and roughness near the mouths of tidal estuaries, elevated production of residual vorticity is expected. An example displayed in Table 1 (Wassaw Channel) and Fig. 3d is the opening of Wassaw Sound onto the South Atlantic Bight. Here tidal flows draining the estuarine system carry a load of fine sediment out to the shelf. A channel 800 m wide is maintained by the tidal currents with a sill of deposited material about 5 km offshore at the seaward extent of the tidal excursion. The flow within the channel experiences a depth change of 3 m over 3 km. The roughness gradient across the side banks is large within the channel [$\Delta z_o/\Delta L_n$ = (1.0–0.5 cm)(500 m)$^{-1}$], but decreases along the tidal excursion path (3 km). The strong cross-channel gradients produce estimated values of residual velocities of 2 cm s^{-1}. The gradient mechanisms are all large and an order of magnitude greater than the Coriolis mechanism.

Seaward of the islands on either side of the entrance to Wassaw Sound are areas of deposited sands. Weakening currents and residual eddies maintain sand deposits like these at the mouth of many rivers and estuaries (Wright 1977). The changes in roughness across these deposits are large. Across the deposits there are fields of sand waves maintained by the surface wave field. The flanks grade into finer clays and silts, which do not maintain distinct ripples. Thus, the z_o value can change by at least a factor of 2 across 3 km, while the depth changes by 10%–20%. The depth gradient mechanism and the roughness gradient mechanism produce similar vorticity with estimated residual velocities of 1 cm s^{-1}. Together the mechanisms may produce residual velocity of 2 cm s^{-1}, which may be partially responsible for the maintenance of this type of roughened bed feature.

6. Conclusions

The residual vorticity generation mechanism by gradients of bottom roughness can be as important as that due to topography. Models that do not resolve subtidal excursion length scales necessarily employ average friction parameters, which subsume all residual vorticity generation mechanisms. These parameterizations cannot yet be based on direct field measurements of topography and roughness. Rather, the match of derived quantities to measurements, such as tidal heights and currents, is used to determine the generalized friction parameters. Until a complete model of the subgrid-scale turbulence and diffusion processes is presented the supragrid parameterizations can be accomplished in no other way.

Alternatively, modeling efforts are attempting to solve the subgrid-scale problems by moving toward finer detail, resolving subtidal length scales. It has been recognized that the unavailability of high-resolution topography charts is a limiting factor. Our scaling of the residual generation mechanisms indicates that charts of equal detail of bottom roughness variation

must also be obtained. The topographic and roughness effects can be of similar magnitude so both must be resolved if progress is to be made past the use of generalized average friction parameterizations.

Acknowledgments. This work was supported by the Office of Naval Research Grant N00014-91-J-1376.

REFERENCES

Abraham, G., and H. Gerritsen, 1990: Sub-grid transport of matter in two-dimensional tidal flow over an uneven bed. *Contin. Shelf Res.*, **10,** 225–242.

——, ——, and G. J. H. Lindijer, 1987: Subgrid tidally induced residual circulations. *Contin. Shelf Res.*, **7,** 285–305.

Backus, R. H., Ed., 1987: *Georges Bank.* The MIT Press, 593 pp.

Cacchione, D. A., D. E. Drake, W. D. Grant, A. J. Williams, and G. B. Tate, 1983: Variability of sea-floor roughness within the Coastal Ocean Dynamics Experiment (CODE) region. WHOI Tech. Rep. 83-25, CODE Tech. Rep. 16a, 44 pp. [NTIS PB90-240532/XAB.]

——, ——, ——, A. J. Williams, and G. B. Tate, 1984: Rippled scour depressions on the inner continental shelf off central California. *J. Sediment. Petrol.*, **54,** 1280–1291.

Field, M. E., J. H. Barber Jr., D. A. Cacchione, D. E. Drake, and F. L. Wong, 1992: U.S. Geological Survey, Open-File Report 92-338, 1 sheet.

Grant, W. D., and O. S. Madsen, 1979: Combined wave and current interaction with rough bottom. *J. Geophys. Res.*, **84,** 1797–1808.

——, and ——, 1982: Movable bed roughness in unsteady oscillatory flow. *J. Geophys. Res.*, **87,** 409–481.

——, and ——, 1986: The continental-shelf bottom boundary layer. *Ann. Rev. Fluid Mech.*, **18,** 265–305.

Gross, T. F., A. E. Isley, and C. R. Sherwood, 1992: Estimation of stress and bed roughness during storms on the northern California shelf. *Contin. Shelf Res.*, **12,** 389–413.

Henry, V. J., 1985: Results of Gray's Reef National Marine Sanctuary hydrographic and geophysical survey. Draft Final Report submitted to Sanctuary Programs Division, Office of Ocean and Coastal Resources Management, NOAA, 53 pp.

Huthnance, J. M., 1973: Tidal current asymmetries over the Norfolk Sandbanks. *Estuarine Coastal Mar. Sci.*, **1,** 89–99.

Jordan, G. F., 1962: Large submarine sand waves. *Science,* **136,** 839–848.

Loder, J. W., 1980: Topographic rectification of tidal currents on the sides of Georges Bank. *J. Phys. Oceanogr.*, **10,** 1399–1416.

Nowell, A. R. M., 1983: The benthic boundary layer and sediment transport. *Rev. Geophys. Space Phys.*, **21,** 1181–1192.

Perry, A. E., W. H. Schofield, and P. N. Joubert, 1969: Rough wall turbulent boundary layers. *J. Fluid Mech.*, **37,** 383–413.

Robinson, I. S., 1981: Tidal vorticity and residual circulation. *Deep-Sea Res.*, **28A,** 195–212.

——, 1983: Tidally induced residual eddies. *Physical Oceanography of Coastal and Shelf Seas,* B. Johns, Ed., Elsevier, 321–356.

Rosenfeld, L. K., and R. C. Beardsley, 1987: Barotropic semidiurnal tidal currents off northern California during the Coastal Ocean Dynamics Experiment (CODE). *J. Geophys. Res.*, **92,** 1721–1732.

Twichell, D. C., B. Butman, and R. S. Lewis, 1987: Shallow structure, surficial geology and the processes currently shaping the Bank. *Georges Bank,* R. H. Backus, Ed., The MIT Press, 31–37.

Wheatcroft, R. A., 1994: Temporal variation in bed configuration and 1-D bottom roughness at the mid-shelf STRESS site. *Contin. Shelf Res.*, in press.

Wieringa, J., 1993: Representative roughness parameters for homogeneous terrain. *Bound.-Layer Meteor.*, **63,** 323–363.

Wooding, R. A., E. F. Bradley, and J. K. Marshall, 1973: Drag due to regular arrays of roughness elements of varying geometry. *Bound.-Layer Meteor.*, **5,** 285–308.

Wright, L. D., 1977: Sediment transport and deposition at river mouths: A synthesis. *Geol. Soc. Am. Bull.*, **88,** 857–868.

Zimmerman, J. T. F., 1978: Topographic generation of residual circulation by oscillatory tidal currents. *Geophys. Astrophys. Fluid Dyn.*, **11,** 35–47.

——, 1981: Dynamics, diffusion and geomorphological significance of tidal residual eddies. *Nature,* **290,** 549–555.